Molecular Therapy
Original Article

Cardiac CIP protein regulates dystrophic cardiomyopathy

Xin He,[1,2,3,11] Jianming Liu,[2,11] Fei Gu,[2] Jinghai Chen,[2,4] Yao Wei Lu,[2] Jian Ding,[2] Haipeng Guo,[2,5] Mao Nie,[2,6] Masaharu Kataoka,[2,7] Zhiqiang Lin,[2] Xiaoyun Hu,[2] Huaqun Chen,[2,8] Xinxue Liao,[1,3] Yugang Dong,[1,3] Wang Min,[1] Zhong-Liang Deng,[2,6] William T. Pu,[2,9] Zhan-Peng Huang,[1,3,10] and Da-Zhi Wang[2,9]

[1]Department of Cardiology, Center for Translational Medicine, Institute of Precision Medicine, The First Affiliated Hospital, Sun Yat-sen University, Guangzhou 510080, China; [2]Department of Cardiology, Boston Children's Hospital, Harvard Medical School, 320 Longwood Avenue, Boston, MA 02115, USA; [3]NHC Key Laboratory of Assisted Circulation (Sun Yat-sen University), Guangzhou, China; [4]Department of Cardiology, Provincial Key Lab of Cardiovascular Research, Second Affiliated Hospital, Zhejiang University School of Medicine, Hangzhou 310009, China; [5]Department of Critical Care and Emergency Medicine, Key Laboratory of Cardiovascular Remodeling and Function Research, Chinese Ministry of Education and Chinese Ministry of Health, Qilu Hospital, Cheeloo College of Medicine, Shandong University, Jinan 250012, China; [6]Department of Orthopaedic Surgery, The Second Affiliated Hospital, Chongqing Medical University, Chongqing, China; [7]Department of Cardiology, Keio University School of Medicine, Tokyo, Japan; [8]Department of Biology, Nanjing Normal University, Nanjing, China; [9]Harvard Stem Cell Institute, Harvard University, Cambridge, MA 02138, USA; [10]National-Guangdong Joint Engineering Laboratory for Diagnosis and Treatment of Vascular Diseases, Guangzhou 510080, China

Heart failure is a leading cause of fatality in Duchenne muscular dystrophy (DMD) patients. Previously, we discovered that cardiac and skeletal-muscle-enriched CIP proteins play important roles in cardiac function. Here, we report that CIP, a striated muscle-specific protein, participates in the regulation of dystrophic cardiomyopathy. Using a mouse model of human DMD, we found that deletion of CIP leads to dilated cardiomyopathy and heart failure in young, non-syndromic *mdx* mice. Conversely, transgenic overexpression of CIP reduces pathological dystrophic cardiomyopathy in old, syndromic *mdx* mice. Genome-wide transcriptome analyses reveal that molecular pathways involving fibrogenesis and oxidative stress are affected in CIP-mediated dystrophic cardiomyopathy. Mechanistically, we found that CIP interacts with dystrophin and calcineurin (CnA) to suppress the CnA-Nuclear Factor of Activated T cells (NFAT) pathway, which results in decreased expression of Nox4, a key component of the oxidative stress pathway. Overexpression of Nox4 accelerates the development of dystrophic cardiomyopathy in *mdx* mice. Our study indicates CIP is a modifier of dystrophic cardiomyopathy and a potential therapeutic target for this devastating disease.

INTRODUCTION

Duchenne muscular dystrophy (DMD) is a genetic disorder caused by mutations in the X-linked dystrophin gene that affects the structure and function of striated muscle (cardiac and skeletal muscle).[1–4] These mutations lead to muscle wasting and regeneration defects in skeletal muscle. Using genome-editing technology, recent studies show that germline or somatic correction of the dystrophin mutation can restore muscle function.[5–9] However, less is known about dystrophic defects in the heart, or dystrophic cardiomyopathy. More than 90% of male DMD patients had cardiac involvement after 18 years of age,[10,11] and dystrophic cardiomyopathy has now become a leading cause of fatality in DMD.[12–15] Most importantly, the pathophysiological mechanisms involved in cardiac myocytes appear to differ significantly from those in skeletal myofibers.[13,16] Therefore, novel therapeutic targets are needed for dystrophic cardiomyopathy.

The pathophysiological conditions of dystrophic cardiomyopathy and the underlying molecular pathways have been investigated in patients and animal models of DMD disease. Loss-of-function dystrophin mutations often result in increased apoptosis, inflammation, oxidative stress, and tissue fibrosis in the heart.[12,13,17,18] It has been shown that alterations in calcium handling and calcineurin (CnA) activation may play a role in dystrophic cardiomyopathy.[17,19–22] An *in vitro* study showed that even physiological mechanical stretch of cardiomyocytes can cause aberrant calcium release in *mdx* mice, an established model of DMD.[17] *In vivo* studies indicated that exercise could activate CnA signaling in the hearts of *mdx* mice,[20] which was associated with exacerbation of dystrophic cardiomyopathy.[19] These data indicated that CnA could be a pathogenic factor at the early stage of dystrophic cardiomyopathy.

We have previously identified CIP as a specifically cardiac and skeletal-muscle-expressed protein.[23] CIP represents alternatively spliced

Received 27 November 2020; accepted 8 August 2021;
https://doi.org/10.1016/j.ymthe.2021.08.022.

[11]These authors contributed equally

Correspondence: Zhan-Peng Huang, PhD, Department of Cardiology, Center for Translational Medicine, Institute of Precision Medicine, The First Affiliated Hospital, Sun Yat-sen University, Guangzhou 510080, China.
E-mail: huangzhp27@mail.sysu.edu.cn
Correspondence: Da-Zhi Wang, PhD, Department of Cardiology, Boston Children's Hospital, Harvard Medical School, 320 Longwood Avenue, Boston, MA 02115, USA.
E-mail: da-zhi.wang@childrens.harvard.edu

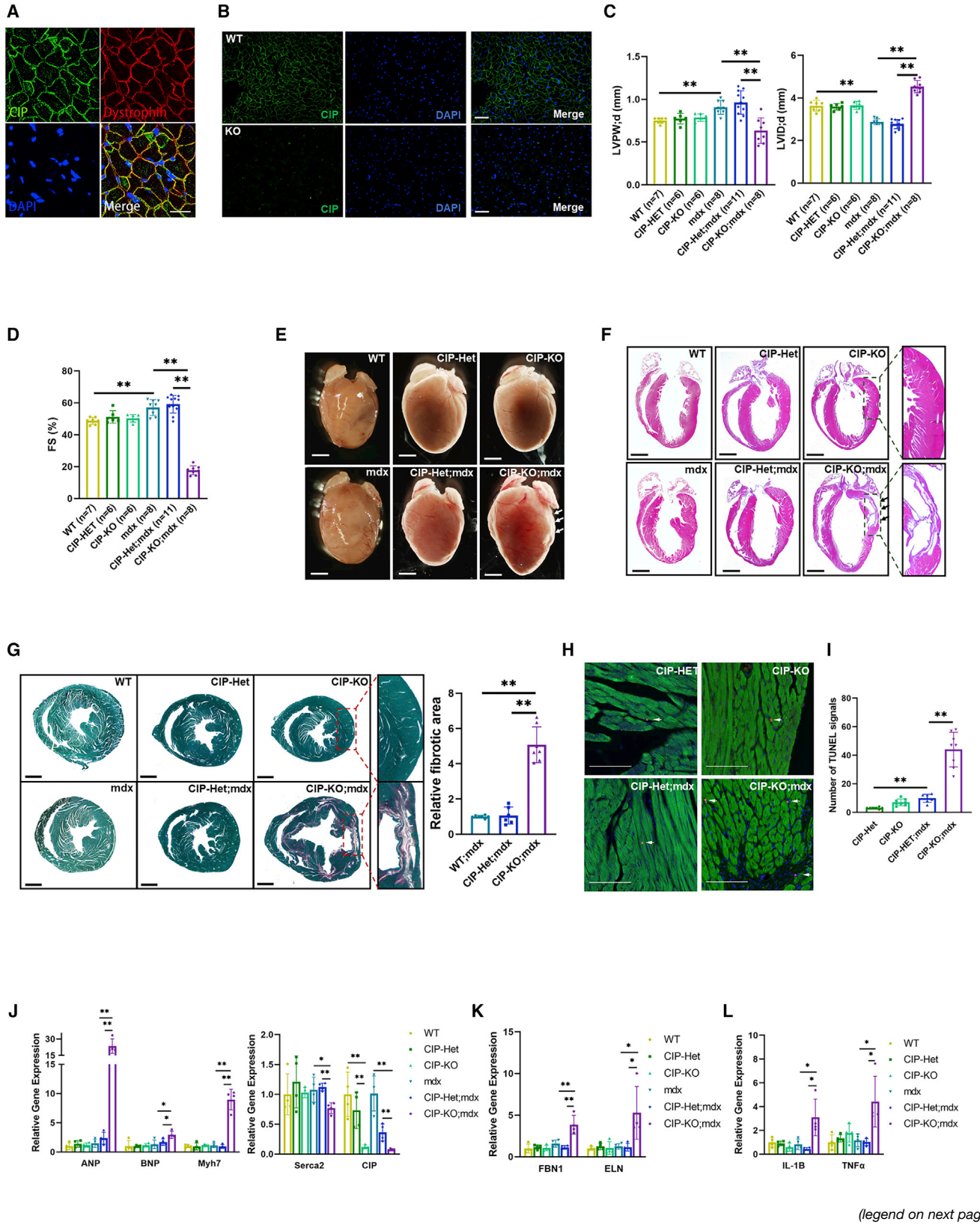

(legend on next page)

isoforms of a recently reported protein called MLIP.[24,25] Most CIP spliced variants contain exons 1, 3, 8, 9, and 10 of full-length MLIP (NM_001368972), with a putative DNA-binding domain located in exons 8 and 9,[23] and have been shown to interact with Lamin A/C.[26] We showed that CIP plays a key role in cardiac remodeling in response to pathophysiological stress.[26] Interestingly, we found that CIP expression was reduced in the heart of CnA transgenic mice and that loss of CIP further accelerated the progression to heart failure in these mice, indicating a functional interaction between CIP and CnA.[26] Importantly, the CIP/MLIP gene is conserved between humans and mice. A recent study linked single-nucleotide variants (SNVs) of human CIP (MLIP) to dilated cardiomyopathy, highlighting the previously unrecognized role of CIP in cardiac disease.[27] However, the molecular mechanism(s) underlying CIP and CnA interactions in the regulation of cardiomyopathy remains elusive.

In the present study, we unexpectedly found that CIP protein is located on the cell membrane of cardiomyocytes, overlapping with dystrophin, which is encoded by the gene that is responsible for muscular dystrophy. We therefore investigated the potential functional involvement of CIP in dystrophic cardiomyopathy. Genetic studies show that loss of CIP accelerates the progression of cardiomyopathy and heart failure in *mdx* mice, a mouse model of human DMD. Most importantly, overexpression of CIP protects the heart from the development of pathological dystrophic cardiomyopathy in *mdx* mice. Mechanistic studies indicate that CIP is associated with dystrophin to repress the CnA-Nuclear Factor of Activated T cells (NFAT) signaling pathway in cardiomyocytes.

RESULTS

Loss of CIP accelerates the development of dystrophic cardiomyopathy

CIP was previously identified as a novel striated muscle enriched protein, which was shown to be located in the nucleus when FLAG-tagged CIP was ectopically expressed in non-myocyte mammalian cells.[23] To better examine the expression and location of endogenous CIP proteins in the heart and skeletal muscle, we generated antibodies that specifically recognize murine CIP proteins. Surprisingly, we noticed that CIP protein is predominantly localized to the cell surface of cardiomyocytes, where it co-localizes with dystrophin (Figure 1A). This CIP protein staining pattern appears to be specific, because the signal is lost in CIP-knockout (KO) hearts (Figure 1B). In contrast, CIP protein is located to the nuclear envelop of skeletal myocytes.[28]

These findings prompted us to test the hypothesis that CIP interacts with dystrophin to modulate muscular dystrophy. We first crossed CIP-KO mice with *mdx* mice, which harbor a dystrophin mutation, to generate a CIP-KO;*mdx* double-knockout (dKO) mouse to test genetic interaction between CIP and dystrophin. CIP-KO mice appear normal without detectable cardiac defects up to 12 months of age,[26] and *mdx* mice only start to display mild cardiomyopathy at 10 months of age.[29–31] Strikingly, we found that the dKO mice exhibit severe cardiomyopathy as early as 3 months of age.

Echocardiographic measurements showed that the left ventricular posterior wall is thinner and the left ventricular internal diameter is enlarged in 3-month-old dKO mice, when compared with control groups (Figure 1C; Table S1). We observed that *mdx* mice at this age exhibit slightly higher fraction shortening; however, the cardiac output of these mice is actually smaller (the difference between LV Vol;d and LV Vol;s) due to abnormal relaxation when compared with that of other control groups (Figures 1C and 1D; Table S1). This observation is consistent with previous observations[32–35] and may reflect hypertrophic remodeling in these mice. Fractional shortening in dKO mice decreased to below 20% (Figure 1D), indicating that they suffer from severe dilated cardiomyopathy and heart failure, which is commonly observed in DMD patients.[12,13] Echocardiography at earlier time points indicated dKO mice started to show systolic dysfunction as early as 9 weeks of age, and cardiac function decreases rapidly between the age of 2 months and 3 months (Table S2).

Morphological and histological examination verified that dKO hearts were significantly enlarged and dilated (Figures 1E and 1F). Intriguingly, the focal myocardial lesions that are often observed in DMD hearts[36] are also found in the left ventricle of dKO hearts but not in control hearts (arrows in Figures 1E and 1F). Sirius red/fast green staining showed a dramatic increase in cardiac fibrosis in dKO hearts (Figure 1G). We examined apoptosis using TUNEL assays and found a dramatic increase in apoptotic cell death in the hearts of dKO mice, although modest apoptosis is also observed in CIP-Het;mdx hearts (Figures 1H and 1I).

We examined molecular markers for cardiomyopathy and heart failure and found that the expression levels of *ANF*, *BNP*, and *Myh7* were all elevated in the hearts of dKO mice (Figure 1J). Notably, the expression of these cardiomyopathy marker genes was not altered in the hearts of control groups (wild type [WT], CIP-Het,

Figure 1. Loss of CIP accelerates dystrophic cardiomyopathy in young *mdx* mice

(A) Immunohistochemistry detecting CIP and dystrophin protein in adult mouse heart sections. Bar, 20 μm. (B) Immunohistochemistry detecting CIP protein in wild-type (WT) and CIP knockout (KO) adult mouse heart sections. Bars, 50 μm. (C) Left ventricular posterior wall thickness at end-diastole (LVPW;d), left ventricular internal dimension at end-diastole (LVID;d), and (D) Fractional shortening (FS) of 3-month-old CIP-KO;*mdx* dKO mice and their control littermates. Compared with WT mice, mdx mice had thicker diastolic LVPW, shorter diastolic LVID, and higher FS, which were similar to the parameters of CIP-HET;mdx mice. Loss of CIP did not alter cardiac function among non-mdx mice but significantly decreased diastolic LVPW, increased diastolic LVID, and decreased FS among mdx mice. (E) Gross heart morphology, and (F) H&E staining of 3-month-old CIP-KO;*mdx* dKO mice and their control littermates. Bars, 1.5 mm. (G) Sirius red/fast green staining of 3-month-old CIP-KO;*mdx* dKO and control hearts. The fibrotic area was quantified. Bars, 1 mm. (H) TUNEL assay of 3-month-old CIP-KO;*mdx* dKO and control hearts. Bars, 50 μm. (I) Numbers of TUNEL signals were quantified. qRT-PCR detection of expression of (J) heart disease marker genes, (K) fibrosis marker genes, and (L) genes related to cell death in 3-month-old CIP-KO;*mdx* dKO hearts and littermate controls. Samples number is indicated by the number of dots in each group in figure panels. The significance between groups was tested with 1-way ANOVA with post hoc Tukey's test. *$p < 0.05$; **$p < 0.01$.

CIP-KO, *mdx*, or CIP-Het;*mdx*), further supporting the view that CIP is specifically involved in the regulation of cardiac function in dystrophic mice. Consistent with increased fibrosis (Figure 1G), we detected increased expression of fibrosis markers *FBN1* and *ELN* in dKO hearts (Figure 1K). In addition, the expression of *IL-1* and *TNF-α*, which are related to cell death and inflammation, was also elevated in dKO hearts (Figure 1L). Collectively, these data indicate that loss of CIP function accelerates disease progression of dystrophic cardiomyopathy.

Transgenic overexpression of CIP protects the heart from the development of dystrophic cardiomyopathy

Next, we asked whether cardiac expression of CIP could protect dystrophic mice from developing cardiomyopathy. We created CIP-overexpressing mice (CIP-OE), in which the CIP transgene is flanked by a floxed Stop codon and is then activated by breeding with MCK-Cre, a Cre recombinase gene driven by the muscle creatine kinase promoter. When bred with mice containing a loxP-flanked sequence of interest, MCK-Cre-mediated recombination will result in skeletal and cardiac muscle CIP overexpression.[37] We bred the CIP-OE with *mdx* mice to create CIP-OE;*mdx* compound mice. CIP-OE mice appear normal, without detectable changes in cardiac function, under physiological conditions. Unlike human DMD patients, *mdx* mice develop mild, late-onset cardiomyopathy.[29,30]

One-year-old *mdx* mice exhibit dilated cardiomyopathy (i.e., enlarged left ventricular chambers, thinner ventricular walls, and enhanced cardiac fibrosis). Cardiac function was preserved in 1-year-old CIP-OE;*mdx* mice compared to their control littermates (Figure 2A; Table S3), indicating that cardiac CIP overexpression blocks the development of cardiomyopathy in *mdx* mice.

Histological analyses revealed dilated ventricular chambers and increased fibrosis in 1-year-old *mdx* mice but no obvious cardiac dilation or fibrosis in 1-year-old CIP-OE;*mdx* mice (Figure 2B). We also examined these mice at earlier and later time points. At 6 months of age, some of the *mdx* mice started to display cardiac dilation and increased fibrosis. In contrast, none of the CIP-OE;*mdx* mice exhibited pathological findings at this age (Figure S1A). By 16 months of age, *mdx* mice displayed severe dilated cardiomyopathy with focal myocardial lesions and fibrosis (arrowhead in Figure S1B), similar to what has been observed in DMD patients.[36] In contrast, there was no ventricular dilation or obvious fibrosis in 16-month-old CIP-OE;*mdx* mice (Figure S1B), indicating that CIP overexpression provides long-term protection from dystrophic cardiomyopathy.

Consistent with the results of functional and cellular analyses, molecular marker gene studies revealed decreased expression of markers of cardiac disease (ANP, BNP) (Figure 2C), fibrosis (FBN1) (Figure 2D), and necrosis (TNF-α) (Figure 2E) in 1-year-old CIP-OE;*mdx* hearts, when compared with controls. Together, these results demonstrate that overexpression of CIP in striated muscle blocks the progression of dystrophic cardiomyopathy in *mdx* mice.

Molecular signature of dystrophic cardiomyopathy

To better define the molecular signature and understand the mechanisms of dystrophic cardiomyopathy, we performed unbiased transcriptome analyses. We isolated RNAs from ventricles of 3-month-old dKO and control *mdx*, because severe cardiac remodeling and fibrosis were observed in these animals. RNA sequencing (RNA-seq) of dKO and control *mdx* hearts (4 hearts from each group) identified 1,891 transcripts that were differentially expressed in CIP-KO;*mdx* hearts, including 855 down- and 1,036 upregulated genes (Figure 3A; Table S4; $p < 0.01$).

Gene Ontology (GO) term analysis revealed that upregulated genes were enriched for functional annotations related to extracellular matrix organization, collagen formation, and integrin signaling. Among the most upregulated genes were genes associated with cardiomyopathy and heart failure (Myh7, NPPA, NPPB, and Acta1) and cardiac fibrosis (collagen genes, Postn, ELN, and tgfb2), consistent with our prior quantitative RT-PCR (qRT-PCR) analyses (Figures 1J and 1K). In contrast, downregulated genes were enriched for functional annotations related to the oxidation-reduction process, oxidoreductase activity, and fatty acid oxidation (Figure 3B). Several transcription factors and co-factors responsible for fatty acid metabolism, including Ppara, Ppargc1a, and Ppargc1b, were downregulated, indicating that they may contribute to the pathology of dystrophic cardiomyopathy.

Given that the severity of cardiac defects in 3-month-old dKO mice and 1-year-old *mdx* mice is similar, and transgenic overexpression of CIP prevented the development of cardiomyopathy in old *mdx* mice, we also performed RNA-seq on 1-year-old CIP-OE;*mdx* and littermate control mice, using total RNAs isolated from ventricles (4 hearts for each group). A total of 791 genes, including 356 up- and 435 downregulated, were dysregulated in CIP-OE;*mdx* hearts when compared with *mdx* controls (Figure 3C; Table S5; $p < 0.05$). Intriguingly, GO term analysis demonstrated inversed molecular signature when compared with 3-month-old CIP-KO;*mdx*, in that the upregulated genes were enriched for functional annotations related to fatty acid catabolic process, fatty acid beta-oxidation, and oxidoreductase activity, while the downregulated genes were enriched for functional annotations related to collagen formation, extracellular matrix organization, and integrin signaling pathway (Figure 3D). These results suggest that cellular processes and molecular pathways for oxidation-reduction and fibrosis are likely key contributors to dystrophic cardiomyopathy.

The RNA-seq data from both young (3-month-old) and aged (1-year-old) mice with various genetic modifications to dystrophin and/or CIP, together with their distinctive pathological conditions, provide a unique opportunity to better understand the molecular signature of dystrophic cardiomyopathy progression. We performed an unbiased principal component analysis (PCA) using the whole transcriptome and found that 1-year-old CIP-OE;*mdx* hearts, which are phenotypically normal, are distant from 1-year-old *mdx* control hearts; instead, their transcriptome signature

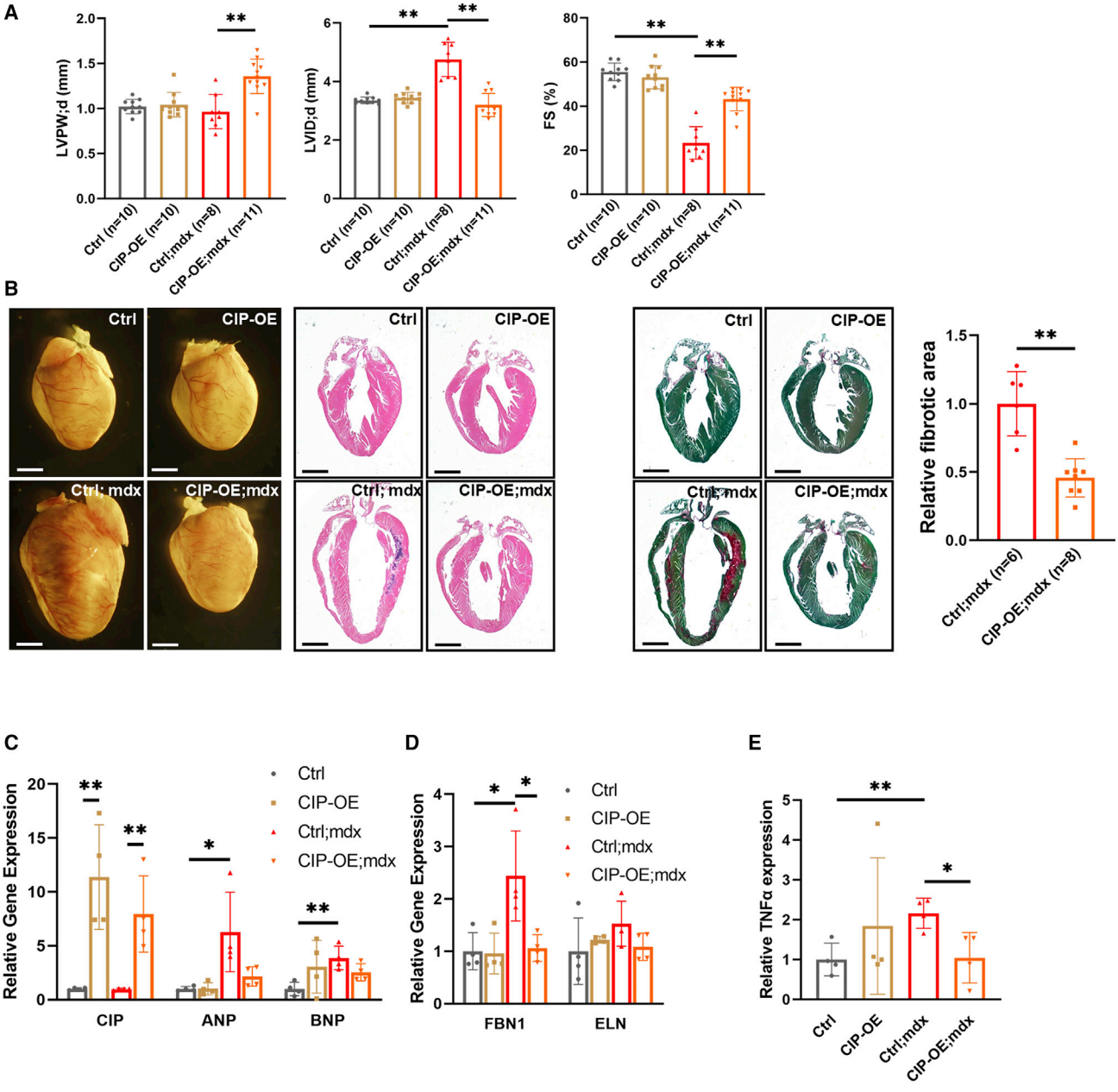

Figure 2. Cardiac overexpression of CIP suppresses dystrophic cardiomyopathy in old *mdx* mice

(A) LVPW;d, LVID;d, and FS of 1-year-old CIP-OE;*mdx* compound mice and controls. (B) Gross heart morphology, H&E staining, and Sirius red/fast green staining of 1-year-old CIP-OE;*mdx* compound mice and controls. Bars, 1.5 mm. The fibrotic area was quantified. N = 6–8. qRT-PCR detection of expression of (C) heart disease marker genes, (D) fibrosis marker genes, and (E) TNF-α gene that is related to cell death in 6-month-old CIP-OE;*mdx* compound hearts and controls. Samples number is indicated by the number of dots in each group in figure panels. The significance between groups was tested with 1-way ANOVA with post hoc Tukey's test. *$p < 0.05$; **$p < 0.01$.

is similar to those of 3-month-old *mdx* controls and other littermate controls (Figure 3E). Conversely, the transcriptome signature of 3-month-old CIP-KO;*mdx* hearts, which exhibit severe cardiomyopathy, is separate from that of 3-month-old *mdx* control hearts, instead grouping with 1-year-old *mdx* control hearts (Figure 3F).

Next, we asked whether the molecular signatures of dysregulated genes could be used to better define dystrophic cardiomyopathy phenotypes in these mice, in which dystrophic cardiomyopathy may or may not be present. Using unsupervised hierarchical clustering to analyze the 791 genes dysregulated in 1-year-old CIP-OE;*mdx* hearts compared with age-matched *mdx* controls, we found that all of the

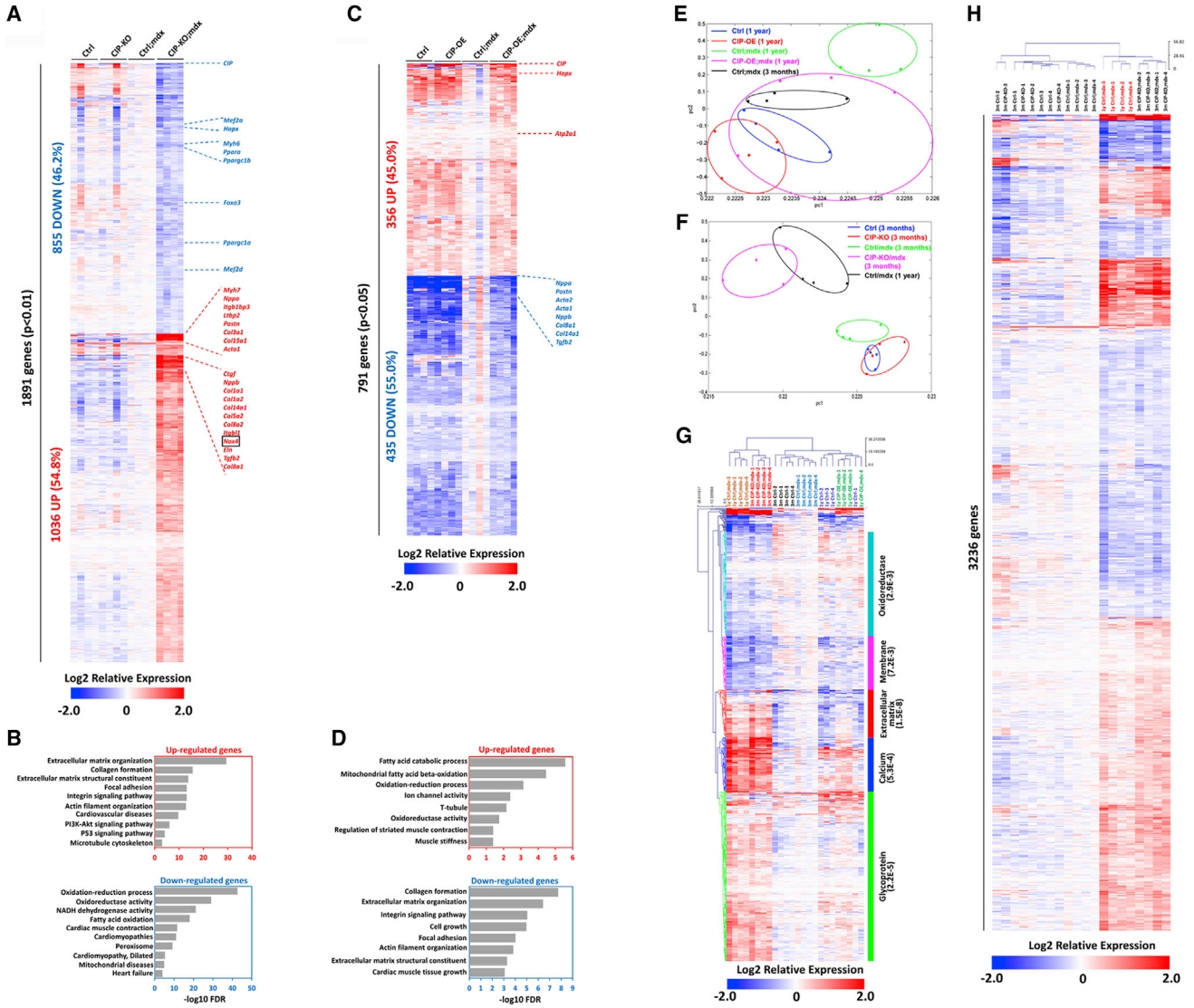

Figure 3. Molecular pathways of dystrophic cardiomyopathy

(A) Heatmap of 1,891 differentially expressed genes in 3-month-old CIP-KO;*mdx* dKO hearts compared to controls ($p < 0.01$). The ctrl;mdx group serves as reference for the heatmap; therefore, the average value of the ctrl;mdx group is 1 (log2 value equal to 0). Each column represents one heart in the heatmap, and N = 4 in each group. (B) Gene ontology analysis of 1,744 upregulated ($p < 0.05$) and 1,492 downregulated ($p < 0.05$) genes in 3-month-old CIP-KO;*mdx* dKO hearts. The Gene Ontology (GO) terms are ranked by false discovery rate (FDR) values. (C) Heatmap of 791 differentially expressed genes in 1-year-old CIP-OE;*mdx* hearts compared to controls ($p < 0.05$). The ctrl;mdx group serves as reference for the heatmap; therefore, the average value of the ctrl;mdx group is 1 (log2 value equal to 0). Each column represents one heart in the heatmap, and N = 4 in each group. (D) Gene ontology analysis of 356 upregulated ($p < 0.05$) and 435 downregulated ($p < 0.05$) genes in 1-year-old CIP-OE;*mdx* hearts. The GO terms are ranked by FDR values. (E) Principal component analysis of all expressed genes in 1-year-old CIP-OE;*mdx* hearts and controls. (F) Principal component analysis of all expressed genes in 3-month-old CIP-KO;*mdx* dKO hearts and controls. In (E) and (F), each dot represents one heart of the indicated genotype. 3-month-old and 1-year-old control;*mdx* data are the same between (E) and (F) and serve as reference transcriptomes of the progression of dystrophic cardiomyopathy. (G) Heatmap from hierarchical clustering of 791 differentially expressed genes in six groups from hearts with the indicated genotypes. Gene clusters from hierarchical classification were subjected to the DAVID web server for GO analysis. Adjusted p value of each GO term is shown. (H) Heatmap from hierarchical clustering of 3,236 differentially expressed genes in 3-month-old CIP-KO;*mdx* dKO and control Ctrl;*mdx* hearts.

1-year-old CIP-OE;*mdx* profiles were separated from 1-year-old *mdx* controls. Instead, they were grouped with 3-month-old *mdx* controls and other littermate controls (Figure 3G).

These molecular signatures are consistent with and further support the results of phenotypic analyses of dystrophic cardiomyopathy mice. These 791 genes are grouped into five clusters, and GO term

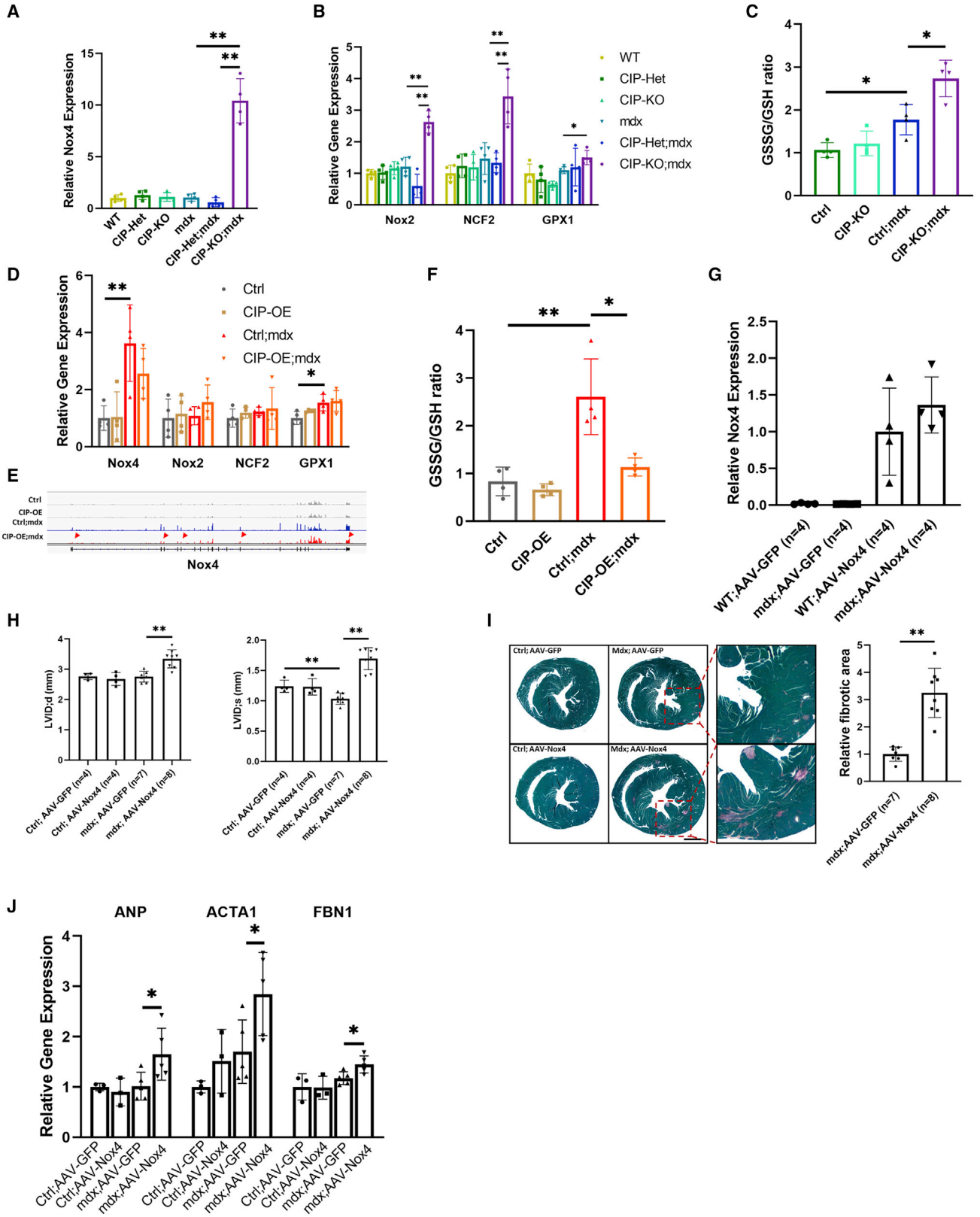

(legend on next page)

analysis of these clusters showed that they were enriched for functional annotations related to Oxidoreductase, Membrane, Extracellular Matrix, Calcium, and Glycoprotein (Figure 3G). Similarly, unsupervised hierarchical clustering of the 3,236 genes dysregulated in 3 month-old CIP-KO;*mdx* hearts compared with age-matched *mdx* controls showed that that the 3-month-old CIP-KO;*mdx* hearts clustered with the 1-year-old *mdx* control hearts (Figure 3H). Together, these analyses uncover a unique molecular signature of dystrophic cardiomyopathy and link the dysregulation of functional gene groups to the pathological condition of this disease.

CIP regulates dystrophic cardiomyopathy and the oxidative stress pathway

Among the most significantly dysregulated gene clusters in dystrophic cardiomyopathy were genes related to extracellular matrix (fibrosis) and the oxidative stress response. We reasoned that increased expression of fibrosis genes in dystrophic CIP-KO;*mdx* hearts and their reduced expression in healthy CIP-OE;*mdx* hearts may represent a consequence of cardiac remodeling. In contrast, we postulate that an increase in the oxidative stress response, as a result of reduced expression of the oxidation-reduction process and oxidoreductase activity genes (Figure 3B), could be a causative factor for dystrophic cardiomyopathy. Importantly, prior studies have shown that oxidative stress, in particular Nox4, plays a critical role in cardiomyopathy.[38–40] We confirmed that the expression of Nox4, an NADPH oxidase, is dramatically upregulated in the heart of 3-month-old CIP-KO;*mdx* dKO mice (Figure 4A). Furthermore, the expression of other oxidases, including Nox2 and NCF2, is also significantly increased in dKO hearts (Figure 4B).

To further confirm an increase in oxidative stress in dKO hearts, we measured the GSSG/GSH ratio, an indicator of oxidative stress,[41] and found it is substantially higher in dKO hearts (Figure 4C). Conversely, we found that the expression of Nox4, but not other oxidases, is reduced in the hearts of 1-year-old CIP-OE;*mdx* mice, when compared with *mdx* mice. However, this decreasing trend is not statistically significant (Figure 4D). To look at Nox4 expression in detail, we examined the RNA-seq data of the distribution of Nox4 expression using the Integrative Genomics Viewer (IGV). As shown in Figure 4E, while increased Nox4 reads are aligned to exons of Nox4 locus of 1-year-old *mdx* hearts when compared with controls, reduced reads were found in 1-year-old CIP-OE;*mdx* hearts compared with *mdx* hearts (arrows in Figure 4E). However, we did not observe a change in other oxidase genes examined, including Nox2, Ncf2, and GPx1 (Figure S2), further supporting the specificity of the response. Consistent with the above observations, we found that the GSSG/GSH ratio increases dramatically in the hearts of 1-year-old *mdx* mice, indicating a significant increase in oxidative stress in aged *mdx* mice. Such increased oxidative stress is rescued by overexpression of CIP in CIP-OE;*mdx* hearts (Figure 4F).

The above data suggested that CIP modulates cardiac oxidative stress in dystrophic hearts, likely by regulating the expression and function of Nox4. Consequently, we asked whether overexpression of Nox4 in the hearts of young *mdx* mice would be able to induce oxidative stress, leading to dystrophic cardiomyopathy, similar to what we saw in CIP-KO;*mdx* dKO mice. We achieved cardiac-specific Nox4 overexpression in *mdx* and control mice using an adeno-associated virus serotype 9 (AAV9) delivery system[26,42–44] (Figure S3). This approach produced comparable Nox4 expression levels in both WT and *mdx* hearts (Figure 4G).

As expected, AAV9-mediated Nox4 overexpression in the hearts of *mdx* mice accelerates cardiac remodeling, resulting in increased systolic and diastolic left ventricle internal dimension (LVID) (Figure 4H). There is also a substantial increase in cardiac fibrosis in Nox4-overexpressed *mdx* mice (Figure 4I). Molecular marker analyses revealed increased expression of ANP and Acta1, both markers of cardiomyopathy, and fibronectin (FBN1), which denotes fibrosis (Figure 4J). In contrast, increased Nox4 expression alone does not alter cardiac dimensions, fibrosis, or marker gene expression in the hearts of the control groups (Figures 4H–4J). Together, these data show that Nox4 accelerates the development of cardiomyopathy in the absence of dystrophin, indicating Nox4 is a critical mediator of dystrophic cardiomyopathy.

CIP interacts with dystrophin and is a component of the dystroglycan complex

Our data demonstrate genetic and functional interaction of CIP and dystrophin in the regulation of cardiac function (Figures 1 and 2). As shown earlier, both CIP and dystrophin proteins are located at the cell membrane of cardiomyocytes (Figure 1A). We asked whether loss of CIP affects the expression of dystrophin transcripts and proteins. Interestingly, dystrophin transcript and protein levels were not affected in the hearts of 2-month-old CIP-KO mice (Figures 5A and 5B). Immunohistochemistry demonstrated that the cellular location of dystrophin was not altered in hearts of adult CIP-KO mice

Figure 4. Oxidative stress and Nox4 are key inducers of dystrophic cardiomyopathy

(A and B) qRT-PCR detection of expression of (A) Nox4, and (B) other oxidative-stress-related genes in 3-month-old CIP-KO;*mdx* dKO hearts and controls. (C) GSSG/GSH ratio in 3-month-old CIP-KO;*mdx* dKO hearts and controls. (D) qRT-PCR detection of the expression of oxidative-stress-related genes in 1-year-old CIP-OE;*mdx* hearts and controls. (E) Integrative Genomics Viewer (IGV) distribution of Nox4 expression as displayed as reads of RNA-seq. Red arrowheads showed that fewer reads were aligned to Nox4 exons in CIP-OE;*mdx* hearts compared to Ctrl;*mdx* hearts. (F) GSSG/GSH ratio in 1-year-old CIP-OE;*mdx* hearts and controls. (G) qRT-PCR detection of Nox4 expression in WT, AAV-Nox4, and *mdx*;AAV-Nox4, and their AAV-GFP controls. (H) LVID;d and LVID;s of 2-month-old *mdx* and control mice injected with AAV-Nox4 or control virus. (I) Sirius red/fast green staining of heart sections of 2-month-old *mdx* and control mice injected with AAV-Nox4 or control virus. The fibrotic area was quantified. Bar, 1 mm. (J) qRT-PCR detection of gene expression in the hearts of 2-month-old *mdx* and control mice injected with AAV-Nox4 or control virus. Samples number is indicated by the number of dots in each group in figure panels. The significance between groups was tested with 1-way ANOVA with post hoc Tukey's test. *$p < 0.05$; **$p < 0.01$.

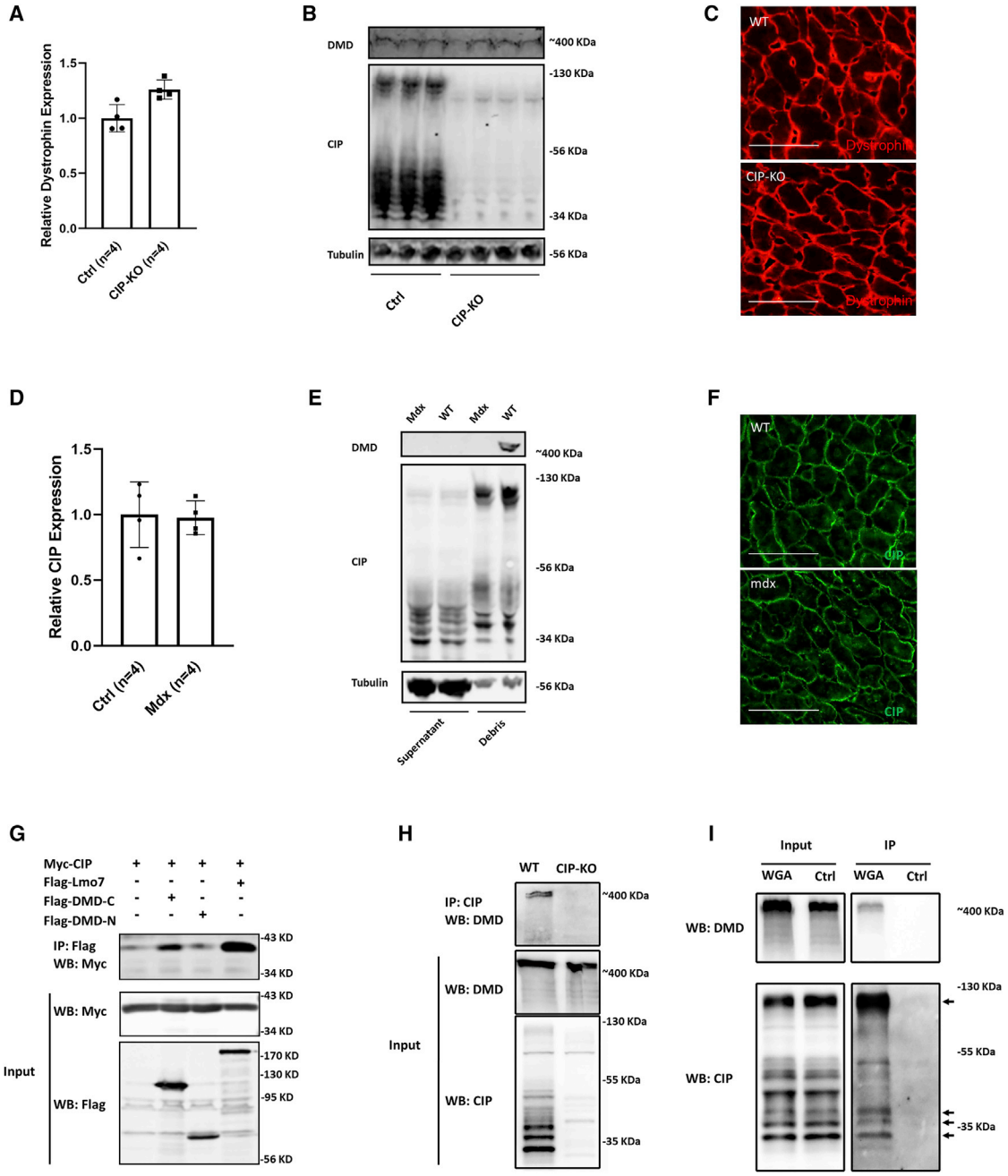

Figure 5. CIP interacts with dystrophin and is a component of the dystroglycan complex

(A) qRT-PCR, and (B) western blot detecting dystrophin mRNA and protein expression in 2-month-old WT and CIP-KO hearts. CIP and β-tubulin proteins serve as controls. (C) Immunohistology detecting dystrophin protein in WT and CIP-KO adult mouse hearts. Bars, 50 μm. (D) qRT-PCR, and (E) western blot detecting CIP mRNA and protein expression in 2-month-old WT and *mdx* mouse hearts. Dystrophin (DMD) and β-tubulin proteins serve as controls. (F) Immunohistology detecting CIP protein in 2-month-old WT and *mdx* hearts. Bars, 50 μm. (G) Coimmunoprecipitation (coIP) assays in HEK293T showing the interaction between Myc-tagged CIP and FLAG-tagged C-terminal of dystrophin (DMD-C) or FLAG-tagged Lmo7, but not FLAG-tagged N-terminal of dystrophin (DMD-N). 5% cell lysate was used as input to demonstrate the expression of tagged proteins. (H) coIP assays using CIP antibodies and protein extracts from WT and CIP-KO hearts showing the interaction of endogenous CIP and dystrophin proteins. 5% tissue lysate was used as input to show indicated proteins. (I) Wheat germ agglutinin (WGA) conjugated or empty (Ctrl) agarose beads were used for pull-down assays of protein extracts from adult WT hearts. Both CIP and dystrophin (DMD) were pulled down by WGA, but not control.

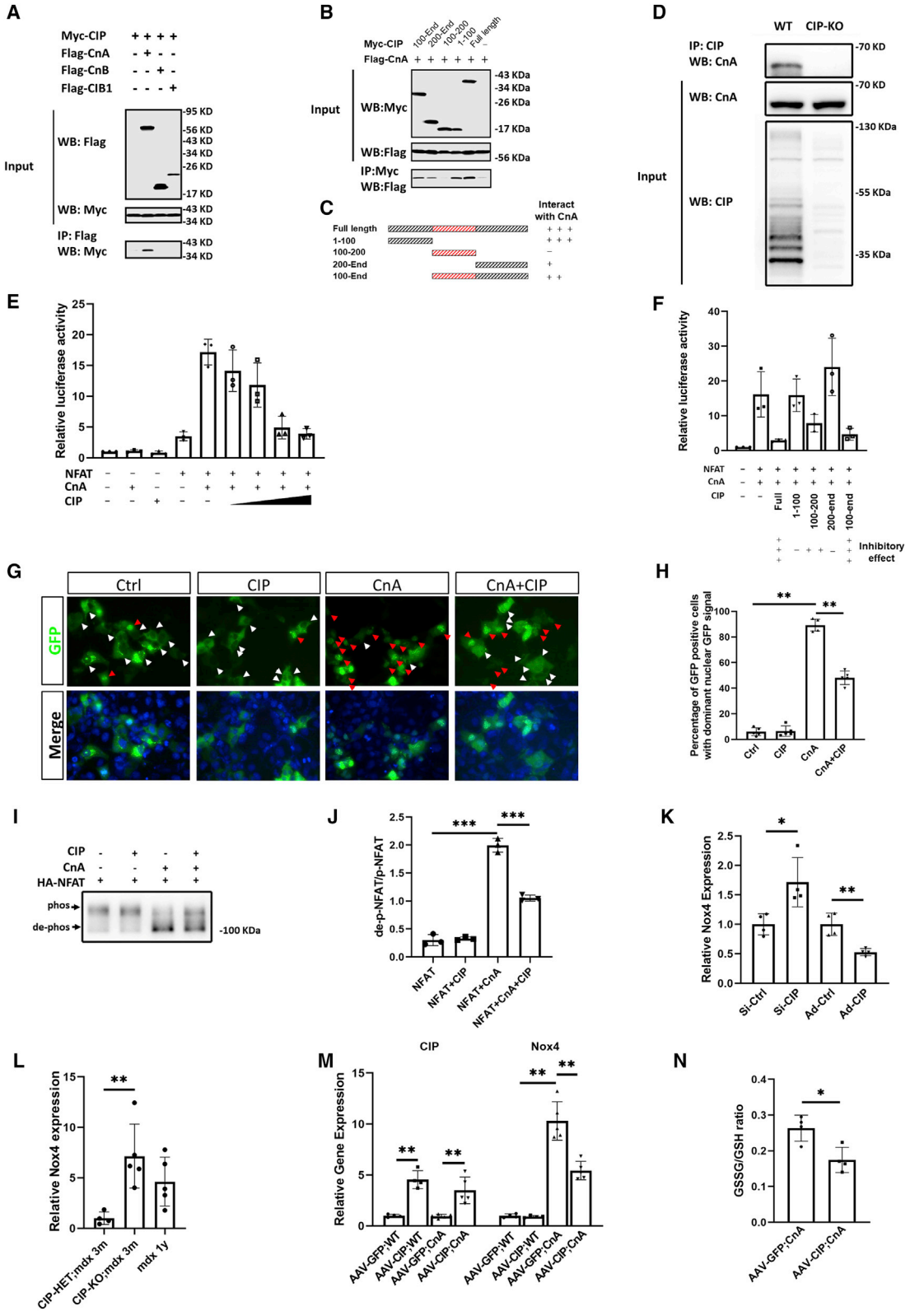

(legend on next page)

(Figure 5C). Conversely, we examined the expression level and location of CIP transcripts and proteins in 2-month-old *mdx* mice and found that loss of dystrophin did not alter the expression levels of CIP (Figures 5D and 5E). The cell membrane location of CIP protein was not changed in cardiomyocytes from *mdx* hearts (Figure 5F). These results suggest that the expression and location of CIP and dystrophin are likely regulated independently, and they do not directly affect each other's expression.

Using co-immunoprecipitation (coIP) assays with tagged proteins, we detected an interaction between CIP and dystrophin. Specifically, CIP could bind the C terminus, but not the N terminus, of dystrophin protein (Figure 5G). Next, we tested whether endogenous CIP and dystrophin proteins interact. Using a CIP-specific antibody to precipitate associated proteins from WT and CIP-KO mice, we found that the CIP antibody pulled down dystrophin from WT hearts, but not CIP-KO hearts (Figure 5H). Given that dystrophin is associated with the dystroglycan complex,[45] we asked whether CIP is also part of the complex. Using wheat germ agglutinin (WGA) to pull down dystroglycan complex proteins from adult hearts, we found that both dystrophin and CIP proteins are pulled down by WGA, but not in controls (Figure 5I). Together, these results suggest that CIP protein is located at the cell membrane of cardiomyocytes and is associated with dystrophin and dystroglycan complex.

CIP interacts with CnA and regulates CnA-NFAT-Nox4 signaling

To better understanding the molecular mechanism by which CIP regulates oxidative stress during dystrophic cardiomyopathy, we undertook an unbiased approach to identify CIP-interacting proteins in the heart. We used GST-CIP to pull down interacting proteins from heart extracts. Subsequent mass spectrometry identified multiple candidate CIP-interacting proteins, including LMO7, HSPA9, α-actinin, β-tubulin, and CnA (CnA). Their interaction with CIP was confirmed by coIP assays (Figure 5G; Figure S4).

CnA is a protein phosphatase that regulates cardiac remodeling.[46–49] We have previously reported that genetic and functional interactions between CnA and CIP modulate cardiac hypertrophy.[26] We therefore tested the potential functional involvement of CnA in CIP-mediated dystrophic cardiomyopathy. coIP assay showed that CIP interacts with CnA, but not CnB or CIB1, a scaffold protein that interacts with CnB and the sarcolemma[50] (Figure 6A). We mapped the domains of the CIP protein that mediate CnA interactions, using deletion constructs in coIP assays. We found that both C- and N-terminal domains of the CIP protein mediate its interaction with CnA (Figure 6B), (summarized in Figure 6C). Furthermore, using a CIP-specific antibody, we immunoprecipitated CIP-associate proteins from adult hearts, and we found that CnA is associated with CIP endogenously. In contrast, no such association is detected from CIP-KO hearts (Figure 6D), demonstrating the specificity of this interaction.

To understand how CIP affects the function of CnA, we used a NFAT-dependent luciferase reporter, in which the expression of the luciferase gene is regulated by NFAT and CnA.[46] We found that overexpression of CIP significantly represses CnA-NFAT-activated NFAT-luciferase activity in a dose-dependent manner (Figure 6E). CIP itself does not affect NFAT-luciferase activity (Figure 6E). Accordingly, CIP protein domains with diminished CnA interaction display reduced ability to inhibit the trans-activity of CnA-NFAT in luciferase reporter assays (Figure 6F). Together, these results suggest that CIP interacts with CnA to modulate its function in the regulation of NFAT activity.

As a transcription factor, NFAT shuttles between the cytoplasm and nucleus, depending on its phosphorylation status. CnA dephosphorylates NFAT to facilitate its nuclear translocation and the activation of downstream cardiac hypertrophic genes.[46] Using an EGFP-tagged NFAT construct, we found that co-transfection of activated CnA potently enhanced the nucleus translocation of NFAT protein (Figure 6G), consistent with a prior report.[51] While overexpression of CIP alone does not affect the subcellular distribution of NFAT, CIP reduces CnA-activated NFAT nuclear translocation (Figure 6G). Quantitative analyses further support this conclusion (Figure 6H). We then asked whether CIP could affect the phosphorylation status

Figure 6. CIP regulates the CnA-NFAT-Nox4 pathway to regulate dystrophic cardiomyopathy

(A) coIP assays in HEK293T showing the interaction between Myc-tagged CIP and FLAG-tagged CnA, but not FLAG-tagged CnB or FLAG-tagged CIB1. 5% cell lysate was used as input to demonstrate the expression of tagged proteins. (B) coIP assays in HEK293T showing interaction between Myc-tagged CIP domains and FLAG-tagged CnA. 5% cell lysate was used as input to demonstrate the expression of tagged proteins. (C) Summary of CIP protein domains that mediate CnA interaction. (D) coIP assays using CIP antibodies and protein extracts from WT and CIP-KO hearts showing an interaction of endogenous CIP and calcineurin A (CnA) proteins. 5% tissue lysate was used as input to show indicated proteins. (E) CIP represses CnA- and NFAT-mediated transactivation of a NFAT-luciferase reporter in a dose-dependent manner. Results are presented as relative luciferase activity, in which the control is assigned a value of 1. Data were generated from at least three independent experiments. (F) CIP and its domains modulate CnA- and NFAT-mediated transactivation of the NFAT-luciferase reporter. Results are presented as relative luciferase activity, in which the control is assigned a value of 1. Data were generated from at least three independent experiments. (G) Green florescence images of Cos-7 mammalian cells co-transfected with EGFP-tagged NFAT and indicated expression plasmids. Nuclei were stained with Hoechst 33342. Red arrows point to cells with nuclear dominant GFP signals, while white arrows point to those cells without nuclear dominant GFP signals. (H) Quantification of the percentage of GFP-positive cells with nuclear dominant GFP signals. (I) HEK293T cells were transfected with CIP, CnA, HA-NFAT as indicated. Western blotting was performed using anti-HA antibody to detect both phosphorylated and de-phosphorylated NFAT protein. (J) Quantification of phosphorylated versus de-phosphorylated HA-NFAT proteins. (K) qRT-PCR detection of Nox4 gene expression in phenylephrine-treated neonatal rat cardiomyocytes when CIP was knocked down (Si-CIP) or overexpressed (Ad-CIP). (L) qRT-PCR detecting Nox4 expression in 3-month-old CIP-HET;*mdx* and CIP-KO;*mdx* and 1-year-old *mdx* hearts. (M) qRT-PCR detection of CIP and Nox4 expression in 4-week-old CnA-tg and control hearts injected with AAV-CIP or control virus. (N) GSSG/GSH ratio in 4-week-old CnA-tg and control hearts injected with AAV-CIP or control virus. Samples number or the number of independent experiments is indicated by the number of dots in each group in figure panels. The significance between groups was tested with 1-way ANOVA with post hoc Tukey's test. *$p < 0.05$; **$p < 0.01$.

of the NFAT protein. We transfected HEK293T cells with CIP, CnA, and hemagglutinin (HA)-NFAT. Western blots demonstrate that CnA significantly increased the ratio of de-phosphorylated and phosphorylated NFAT proteins (de-p-NFAT/p-NFAT), as previously reported,[52,53] and CIP markedly reduced the de-p-NFAT/p-NFAT ratio (Figures 6I and 6J).

A previous study showed that the CnA-NFAT signaling cascade regulates the expression and function of oxidases Nox4 and Nox2 in the kidney.[54] Therefore, we hypothesized that the interplay of CIP, CnA, and dystrophin might modulate downstream oxidative stress and, as a result, the development of dystrophic cardiomyopathy. We used an adenovirus system to overexpress CIP (Ad-CIP) in neonatal rat ventricular myocytes (NRVMs). Cells were treated with phenylephrine (PE) to activate the CnA-NFAT signaling and induce cardiomyocyte hypertrophy.[55,56] Indeed, CIP overexpression results in reduced Nox4 levels when compared with Ad-Ctrl (Figure 6K). Conversely, small interfering RNA (siRNA)-mediated knockdown of CIP results in increased Nox4 expression in NRVMs treated with PE (Figure 6K).

Lastly, we examined how CIP and CnA regulate Nox4 expression and oxidative stress in the heart *in vivo*. We first compared Nox4 expression in 3-month CIP-KO;*mdx* and 1-year *mdx* hearts and found a trend of higher Nox4 expression in 3-month CIP-KO;*mdx* hearts compared to 1-year *mdx* hearts (Figure 6L). We then used AAV9-mediated overexpression of CIP in the hearts of both WT and CnA transgenic mice with AAV9-GFP as a control. AAV9-CIP had little impact on Nox4 expression in WT hearts; however, CIP markedly repressed CnA-induced Nox4 levels in the hearts of CnA transgenic mice (Figure 6M). As a result, the GSSG/GSH ratio is decreased in CIP overexpressed CnA transgenic hearts, when compared with controls (Figure 6N). These data suggest that CIP regulates oxidative stress in cardiomyocytes during cardiac remodeling through the CnA-NFAT-Nox4 signaling cascade.

DISCUSSION

Our study demonstrates that cardiac-expressed CIP participates in the regulation of cardiac function in the dystrophic heart, at least in part, through modulation of the expression and function of Nox4 and oxidative stress by regulating the CnA-NFAT pathway. We further reveal that increased oxidative stress is a key factor in dystrophic cardiomyopathy. This study identifies CIP as a new modifier of dystrophic cardiomyopathy and suggests it could become a therapeutic target to treat this disease.

Loss of dystrophin, an important structural protein on the plasma membrane of cardiac and skeletal muscle cells, leads to an increase in cell permeability, fibrosis, and inflammatory responses of myocytes and eventually results in loss of myocytes and a decrease of muscle contractility.[12,13,57–59] This creates a substantial challenge for the potential treatment of muscular dystrophy.[3,60,61] The pathophysiology and cell biology of muscular dystrophy, including that of cardiomyopathy and heart failure, has been extensively investigated. However, the underlying molecular signature and mechanisms remain to be fully understood. Here, we have created unique mouse models that exhibit many features of dystrophic cardiomyopathy, and our gene expression signature analyses revealed molecular pathways closely associated with the conditions of dystrophic cardiomyopathy, confirming previous reports.[36,62]

There have been several studies providing data on transcriptomic changes in dystrophic cardiomyopathy. Chevalier et al.[63] reported on the transcriptome of isolated cardiomyocytes from *mdx* mice between the ages of 8 and 15 weeks, where they found only minimal changes. This finding is not totally surprising, because the heart samples were collected much earlier than the timing associated with changes to the cardiac phenotype. Rogers et al.[64] provided RNA-seq data of approximately 1-year-old female *mdx* mice. They found that the extracellular matrix was the most enriched cell component in gene ontology analyses, consistent with our findings from 3-month-old dKO and 1-year-old *mdx* hearts. Kamdar et al.[65] compared the single-cell transcriptome of human-induced pluripotent stem cell-derived cardiomyocytes (hiPSC-derived CMs) from DMD patients and unaffected controls. They found that the fibrosis program was more activated in the hiPSC-derived CMs from DMD patients. With the analysis of transcriptome dynamics of dystrophic hearts from non-syndromic stage to syndromic stage and dystrophic hearts with manipulation of CIP expression, our data support the view that dystrophic cardiomyopathy is associated with a unique transcriptome landscape, which will enable a better design for future therapeutic interventions.

Although not all the dysregulated genes identified from RNA-seq were directly regulated by CIP, the most significantly dysregulated genes in CIP-KO;*mdx* and CIP-OE;*mdx* mice were also related to the extracellular matrix in our study. Data from the present and previous studies support the concept that cardiac fibrosis is likely a "default" end point of dystrophic cardiomyopathy.[12,36,61,66,67] This change in fibrosis-related genes supports that CIP-KO or CIP-OE alters progression of dystrophic cardiomyopathy.

Our results show that genes involved in the fatty acid oxidation and oxidation-reduction process were dysregulated in the hearts of syndromic 3-month-old CIP-KO/*mdx* dKO and 1-year-old *mdx* mice, represented by the downregulation of Ppara and upregulation of Nox4. These results were in line with previous findings related to metabolic remodeling and oxidative stress in dystrophic cardiomyopathy.[62,68,69]

Numerous studies have linked the oxidative stress pathway to cardiomyopathy.[70,71] Reactive oxygen species (ROS) have an important physiologic role in normal cardiomyocytes.[70] Prosser et al.[17] showed that ROS could mediate stretch-induced calcium release and, therefore, cardiomyocyte contraction. Abnormal production of ROS in diseased cardiomyocytes, such those found in the *mdx* hearts, could contribute to oxidative stress and disease progression.[17] While Nox4 is the major source of ROS in the heart,[39] the effect of Nox4 in the heart remains controversial.[71] Two independent studies drew opposite conclusions using Nox4 KO and overexpression approaches

in response to pressure overload.[39,72] Although several studies found dysregulated Nox4 expression in dystrophic hearts,[62,66,69] the specific role of Nox4 in dystrophic cardiomyopathy has not been established.

Our study provides evidence to demonstrate that ectopic overexpression of Nox4 in *mdx* mice activates the oxidative stress pathway and leads to cardiomyopathy. Future studies, using loss-of-function approaches, will be needed to more definitively determine if Nox4 is required for the development of dystrophic cardiomyopathy and, if so, whether Nox4 inhibition can become an effective therapy for heart failure in muscular dystrophy patients.

Activation of CnA could be an early pathogenic event in dystrophic cardiomyopathy.[73–75] Calcineurin was upregulated in hearts from young *mdx* mice, before an apparent cardiomyopathy phenotype is manifest.[20] However, how this signaling factor is regulated in heart is still not fully understood. Our previous study indicated that there was a synergistic effect between CIP-KO and CnA overexpression;[26] however, the molecular mechanisms underlying the genetic and functional interaction of these two proteins remain to be fully explored. In the present study, our data support a mechanistic model that CIP could form a complex with CnA in cardiomyocytes and modulate the action of CnA on the downstream NFAT pathway, leading to a reduction of nuclear translocation of de-phosphorylated NFAT proteins and the repression of Nox4 expression, which warrants further testing *in vivo* using genetic engineering.

Previous studies have suggested that in DMD patients, the pathophysiological mechanisms involved in cardiac myocytes seem to differ significantly from those in skeletal myofibers.[12,13] Intriguingly, we also observed that a skeletal-muscle-specific CIP isoform, skCIP, regulates myonuclear positioning in skeletal myoblasts and myotubes, thereby modulating skeletal muscle function and regeneration.[28] Together with the results reported here, our findings indicate that cardiac and skeletal-muscle-specific CIP isoforms participate in the regulation of myocyte function in the heart and skeletal muscle through different mechanisms. CIP is an important regulator of cardiac remodeling and function and appears to be a novel modifier of dystrophic cardiomyopathy. Given that a recent study found that human CIP was mutated in patients with dilated cardiomyopathy and heart failure,[27] CIP could be a novel target for therapeutic treatment of dystrophic cardiomyopathy. With the continued improvement of transgene delivery, such as the AAV system, the CIP transgene could be specifically delivered to heart to treat dystrophic cardiomyopathy in the near future.

MATERIALS AND METHODS

Mice

All experimental procedures involving animals in this study were reviewed and approved by the Institutional Animal Care and Use Committee at the Boston Children's Hospital. CIP-KO and CIP-KI-flox mice were described previously[26] and bred with *mdx* mice.[76] To obtain CIP-OE mice, the CIP-KI-flox mice, which have a Rosa-CIP allele (containing a loxed stop codon) were bred with MCK-Cre mice[37] to excise the stop codon and activate the CIP transgene in the heart and skeletal muscle. Calcineurin transgenic mice (CnA-tg)[46] were used in this study. All compound *mdx* mice used in this study are males, which are offspring of the mating between CIP-KO (males) with CIP-Het;DMD-Het (females) or CIP-KI$^{F/F}$;MCK-Cre (males) with CIP-KI$^{F/F}$;DMD-Het (females). Compound mutant mice on mixed genetic backgrounds were used, and all comparisons used littermates as controls.

Measurement of cardiac function by echocardiography

Echocardiographic measurements were performed on mice using a Visual Sonics Vevo 2100 Imaging System (Visual Sonics, Toronto, ON, Canada) with a 40 MHz MicroScan transducer (model MS-550D). Mice were anesthetized with isoflurane (2.5% isoflurane for induction) and fastened on the platform. Then the supply of isoflurane was stopped to wait for the awakening of mice. The echocardiographic data were captured when the heartbeat returned to ~600 beats per minute. Heart rate and left ventricular (LV) dimensions, including diastolic and systolic wall thicknesses and LV end-diastolic and end-systolic chamber dimensions were measured from two-dimensional (2D) short axis under M-mode tracings at the level of the papillary muscle. LV mass and functional parameters such as percentage of fractional shortening (FS%) and ejection fraction (EF%) were calculated using the above primary measurements and accompanying software. Data from at least 5 animals were collected for each group.

Generation and administration of AAV9

GPF-tagged mouse CIP cDNA, FLAG-tagged mouse Nox4 cDNA, and GFP were separately cloned into inverted terminal repeats (ITR)-containing AAV plasmid (Penn Vector Core P1967) harboring the chicken cardiac TNT promoter, to yield the constructs pAAV9-cTnT-CIP, pAAV9-cTnT-Nox4, and pAAV9-cTnT-GFP, respectively. AAV was packaged using AAV9:Rep-Cap and pAd:deltaF6 (Penn Vector Core) as described.[77] AAV9 was packaged in 293T cells with AAV9:Rep-Cap and pAd deltaF6, then purified and concentrated by gradient centrifugation. AAV9 titer was determined by qPCR. AAV9 virus (4×10^{11} virus genome/animal) were injected into postnatal day 2 CnA-tg pups, *mdx* pups, or their control littermates with subcutaneous injection. Hearts were harvest at the age of 4 weeks for CnA-tg mice and at the age of 2 months for *mdx* mice. At least 4 mouse hearts were studied in each group.

Hematoxylin and eosin (H&E) staining and Sirius red/fast green collagen staining.

Mouse heart tissues were dissected out, rinsed with PBS, and fixed in 4% paraformaldehyde (pH 8.0) overnight. After dehydration through a series of ethanol baths, samples were embedded in paraffin wax according to standard laboratory procedures. Sections of 5 μm were stained with H&E for routine histological examination with light microscope. For Sirius red/fast green collagen staining, sections were fixed with pre-warmed Bouin's solution, 55°C, for 1 h then washed in running water. Sections were stained in 0.1% fast green solution for 10 min, then washed with 1% acetic acid for 2 min. After rinsing

in tap water, sections were stained in 0.1% Sirius resolution for 30 min. After staining, sections were dehydrated and cleared with xylene. The images were examined with light scope and quantified with ImageJ software. Data from at least 5 animals were collected for each group.

Immunofluorescence

Mouse heart tissues were dissected out, collected, and fixed in 4% paraformaldehyde (PFA) at 4°C for 4 h. After washing in PBS, samples were treated in 15% and 30% sucrose for 2 h each and embedded in optical cutting temperature (OCT). About 5–8 μm cryostat sections were collected on positively charged slides. Sections were washed in PBS, blocked in 5% serum/PBS, and subjected to immunostaining. Antibody sources were as follows: anti-CIP (1:500, 21st Century Biochemical, customized), anti-dystrophin (1:500, Sigma-Aldrich D8168), anti-FLAG (1:200, Sigma-Aldrich, F1804), and Alexa 488 and 594 secondary antibodies (Life Technologies). Fluorescently stained cells were counterstained with DAPI and imaged with an FV1000 confocal microscope (Olympus).

Cardiomyocyte culture

Neonatal rat cardiomyocytes were prepared as previously described.[78] Briefly, neonatal cardiomyocytes were isolated by enzymatic disassociation of 1-day-old neonatal rat heart with the Neonatal Cardiomyocyte Isolation System (Cellutron Life Technology). Cardiomyocytes were plated for 2 h to remove fibroblasts. Cells were then plated on 1% gelatin-coated plates in medium containing 10% horse serum and 5% fetal calf serum (FCS). 18 h after plating, cells were changed into serum-free medium and infected with adenovirus (25 MOI) for 24 h. For the treatment of siRNA, 50 nM of siRNA targeting CIP transcript (Si-CIP) and control siRNA (Dharmacon) were transfected into cardiomyocytes by using Lipofectamine RNAiMAX transfection reagent. 6 h later, medium with transfection reagent was removed. Cells were then treated with PE (20 μM). Cells were harvested 24 h after PE treatment for RNA isolation or 4 h after PE treatment for measurement of GSH/GSSG ratio.

qRT-PCR and western blot analysis

Total RNAs were isolated using Trizol Reagent (Life Technologies) from cells and tissue samples. For qRT-PCR, 2.0 μg RNA samples were reverse-transcribed to cDNA by using random hexamers and MMLV reverse transcriptase (Life Technologies) in 20 μL reaction. In each analysis, 0.1 μL cDNA pool was used for qPCR. The relative expression of interested genes is normalized to the expression of 18S rRNA or β-actin. Data from at least 4 animals or from 3 independent cell-cultured experiments were collected for each group. For western blot analyses, protein samples were cleared by 10,000 × *g* centrifugation for 10 min. Samples were subsequently analyzed by SDS/PAGE and transferred to polyvinylidene fluoride (PVDF) membranes that were incubated with Odyssey Blocking Buffer (LI-COR Biosciences) and anti-CIP (1:2,000, 21st Century Biochemical, customized), anti-β-tubulin (1:10,000, Sigma-Aldrich, T0198), anti-FLAG (1:5,000, Sigma-Aldrich, F7425), anti-Myc (1:5,000, Sigma-Aldrich, C3956), anti-Lmo7 (1:1,000, Santa Cruz Biotechnology, sc-376807), anti-HSPA9 (1:1,000, Santa Cruz Biotechnology, sc-133137), anti-α-actinin (1:1,000, Sigma-Aldrich, A7811), anti-calcineurin A (1:1,000, Cell Signaling Technology, 2614), or anti-dystrophin (1:1,000, Sigma-Aldrich, D8168) overnight at 4°C and then washed three times with PBS buffer before adding IgG secondary antibody. Specific protein bands were visualized by Odyssey CLx imager (LI-COR).

CoIP assays

HEK293T cells were transiently transfected with plasmids using Lipofectamine 3000 (Invitrogen). Cells were harvested 48 h after transfection in lysis buffer composed of PBS containing 0.5% Triton X-100, 1 mM EDTA, 1 mM phenylmethylsulfonyl fluoride (PMSF), and complete protease inhibitors (Roche). For heart tissue, neonatal CIP-KO and control hearts were lysed with above-mentioned lysis buffer. After a brief sonication and removal of debris by centrifugation, proteins were precipitated with anti-FLAG, anti-Myc, or anti-CIP antibodies and protein A/G beads and analyzed by western blotting with indicated antibodies. For endogenous coIP, heart protein from 8- to 12-week-old WT or CIP-KO mice was harvested in lysis buffer (50 mM Tris [pH 7.4], 150 mM NaCl, 1% NP-40, 0.25% sodium deoxycholate) (Beyotime) with complete protease inhibitors (Roche). The lysates were briefly sonicated and then incubated with anti-CIP antibody at 4°C overnight. Protein A/G beads were added to the solution, which was incubated at 4°C for another 1 h. Beads were washed by lysis buffer for 30 min 4 times, boiled in 2× loading buffer and analyzed by western blotting.

WGA pull-down assays

Heart protein from 8- to 12-week-old WT or CIP-KO mice was harvested in lysis buffer (50 mM Tris [pH 7.4], 150 mM NaCl, 1% NP-40, 0.25% sodium deoxycholate) (Beyotime) with complete protease inhibitors (Roche). The lysates were briefly sonicated and then incubated with WGA-conjugated agarose beads (Sigma-Aldrich) or empty agarose beads (Solarbio) at 4°C overnight. Beads were washed by lysis buffer for 30 min 4 times, boiled in 2× loading buffer, and analyzed by western blotting.

In vitro GST protein-binding assays

Plasmids encoding a GST fusion with CIP were transformed into BL21 plus cells (Stratagene). The cells were grown at 37°C in 2× YT medium to an optical density of 1.0. Isopropyl-β-D-thiogalactopyranoside (50 μM) was then added to the culture to induce protein expression. After being shaken at room temperature for 4 h, the cells were harvested, and the GST protein was purified with glutathione beads. Glutathione beads conjugated with GST fusion protein were incubated with wild-type heart lysate at 4°C for 6 h in 500 μL of GST-binding buffer (20 mM Tris [pH 7.3]/150 mM NaCl/0.5% Nonidet P-40/protease inhibitor/1 mM PMSF). The beads were washed three times with GST binding buffer. 25 μL of SDS loading buffer was then added to the beads. After boiling, 25 μL was loaded onto an SDS/PAGE gel to separate the CIP-binding proteins. Gel was then stained with Coomassie blue. Stained protein bands were cut out and followed by mass spectrometry analysis.

Constructs, cell culture, and luciferase reporter assays

COS7 and HEK293T cells were cultured in DMEM supplemented with 10% FBS in a 5% CO_2 atmosphere at 37°C. Firefly luciferase reporter constructs fused with the 3× NFAT binding sequence in the upstream region were purchased from Addgene. Transfections were performed with Lipofectamine 3000 (Invitrogen) reagents according to the manufacturer's instruction. Cells were co-transfected with NFAT luciferase reporter, Renilla luciferase reporter (normalizing control), and other indicated plasmids. 48 h after transfection, cell extracts were prepared, and luciferase activity was determined. For luciferase assay, normalized luciferase activity from triplicate samples in 12-well plates relative to Renilla luciferase activity was calculated, and the results are expressed as fold activation over the value relative to the control (NFAT luciferase reporter and empty pcDNA). To determine the subcellular location of GFP-NFAT fusion protein, COS7 cells were co-transfected with GFP-tagged NFAT plasmid (Addgene) and other indicated plasmids. Cells were cultured for 24 h before taking the live cell images.

NFAT dephosphorylation assays

As shown by previous studies, phosphorylation of NFAT could slow down its migration during electrophoresis, which made it possible to differentiate the phosphorylated and dephosphorylated protein by western blotting.[52,53] pcDNA-CIP, pcDNA-CnA, pcDNA-HA-NFAT, and empty pcDNA (to normalize the total plasmid amount) were transfected into HEK293T cells. Cell proteins were harvested in RIPA (Beyotime) 48 h after transfection, briefly sonicated, and analyzed by western blotting with anti-HA antibody.

GSH/GSSG measurement

Measurement of GSH/GSSG was performed with GSH/GSSG Ratio Detection Assay Kit (ab138881) according to manufacturer's instruction. Data from 4 hearts were collected for each group.

RNA-seq data analysis

Raw reads were mapped to UCSC mm9 using Tophat 2.0.[79] RNA fragment was counted by htseq-count.[80] RNA fragment was further normalized per kilobase of exon per million mapped fragment (FPKM). Differentially expressed gene was calculated using DEseq,[81] and fold change > 0.5 and p value < 0.05 were used as parameters. Data from 4 hearts were collected for each group.

Heatmap of gene expression level

Log2 fold change was calculated by fragments in treated groups over control groups. A positive value stands for higher expression level in treated groups and vice versa. The heatmap was clustered using the hierarchy cluster method, and for the Euclidean distance, complete linkages were used as the parameter.

Principal component analysis

All expressed genes in the genome from RNA-seq analyses were used as the signature of each group. Principal component analysis method was used to find top principal components among groups. We found that the top 2 principal components were sufficient to reach a cumulative energy of 0.98. Principal components 1 and 2 were plotted as x axis and y axis in 2D coordinates.

Statistics

Values are reported as means ± STD unless indicated otherwise. An analysis of variance (ANOVA) followed by Tukey's testing was used to evaluate the statistical significance for multiple-group comparisons. In addition, the 2-tailed Mann-Whitney U test was used for 2-group comparisons. Values of $p < 0.05$ were considered statistically significant.

SUPPLEMENTAL INFORMATION

Supplemental information can be found online at https://doi.org/10.1016/j.ymthe.2021.08.022.

ACKNOWLEDGMENTS

We thank members of the Wang and Huang laboratories for advice and support. We thank F. Wang and D.B. Cowan for critical reading of the manuscript. This work is supported by the NIH (HL085635, HL116919, and HL125925) and the Muscular Dystrophy Association (294854) to D.-Z.W. J.L. is supported by the NIH (T32HL007572) and the Muscular Dystrophy Association (186548). Z.-P.H. is supported by the National Natural Science Foundation of China (81873463), an American Heart Association Scientist Development Grant (16SDG29760000), the Guangdong Basic and Applied Basic Research Foundation (2019B151502003), and the Guangdong Science and Technology Department (2018A050506026). M.K. was supported by Banyu Life Science Foundation International.

AUTHOR CONTRIBUTIONS

X. He, Z.-P.H., J.L., and D.-Z.W. conceived the project, designed the experiments, analyzed the data, and wrote the manuscript. X. He, Z.-P.H., J.L., J.D., and H.G. performed molecular biology experiments. Z.-P.H., M.K., and J.C. contributed to the echocardiographic data acquisition and analysis. Z.-P.H., J.D., and Z.L. contributed to adeno-associated virus preparation and administration. X. He, Z.-P.H., M.N., J.L., X. Hu, and H.C. contributed to the histological and immunofluorescent data acquisition and analysis. Z.-P.H. and F.G. performed RNA-seq experiments and data analysis. W.T.P. supervised the CIP-KO mice generation and reviewed the manuscript. All other authors were involved in technical support and discussion of the data.

DECLARATION OF INTERESTS

The authors declare no competing interests.

REFERENCES

1. Hoffman, E.P., Brown, R.H., Jr., and Kunkel, L.M. (1987). Dystrophin: the protein product of the Duchenne muscular dystrophy locus. Cell *51*, 919–928.

2. Monaco, A.P., Neve, R.L., Colletti-Feener, C., Bertelson, C.J., Kurnit, D.M., and Kunkel, L.M. (1986). Isolation of candidate cDNAs for portions of the Duchenne muscular dystrophy gene. Nature *323*, 646–650.

3. Chamberlain, J.R., and Chamberlain, J.S. (2017). Progress toward Gene Therapy for Duchenne Muscular Dystrophy. Mol. Ther. *25*, 1125–1131.

4. Guiraud, S., and Davies, K.E. (2017). Pharmacological advances for treatment in Duchenne muscular dystrophy. Curr. Opin. Pharmacol. *34*, 36–48.

5. Long, C., Amoasii, L., Mireault, A.A., McAnally, J.R., Li, H., Sanchez-Ortiz, E., Bhattacharyya, S., Shelton, J.M., Bassel-Duby, R., and Olson, E.N. (2016). Postnatal genome editing partially restores dystrophin expression in a mouse model of muscular dystrophy. Science *351*, 400–403.

6. Long, C., McAnally, J.R., Shelton, J.M., Mireault, A.A., Bassel-Duby, R., and Olson, E.N. (2014). Prevention of muscular dystrophy in mice by CRISPR/Cas9-mediated editing of germline DNA. Science *345*, 1184–1188.

7. Min, Y.L., Bassel-Duby, R., and Olson, E.N. (2019). CRISPR Correction of Duchenne Muscular Dystrophy. Annu. Rev. Med. *70*, 239–255.

8. Amoasii, L., Hildyard, J.C.W., Li, H., Sanchez-Ortiz, E., Mireault, A., Caballero, D., Harron, R., Stathopoulou, T.R., Massey, C., Shelton, J.M., et al. (2018). Gene editing restores dystrophin expression in a canine model of Duchenne muscular dystrophy. Science *362*, 86–91.

9. Hakim, C.H., Wasala, N.B., Nelson, C.E., Wasala, L.P., Yue, Y., Louderman, J.A., Lessa, T.B., Dai, A., Zhang, K., Jenkins, G.J., et al. (2018). AAV CRISPR editing rescues cardiac and muscle function for 18 months in dystrophic mice. JCI Insight *3*, e124297.

10. Nigro, G., Comi, L.I., Politano, L., and Bain, R.J. (1990). The incidence and evolution of cardiomyopathy in Duchenne muscular dystrophy. Int. J. Cardiol. *26*, 271–277.

11. Meyers, T.A., and Townsend, D. (2019). Cardiac Pathophysiology and the Future of Cardiac Therapies in Duchenne Muscular Dystrophy. Int. J. Mol. Sci. *20*, 4098.

12. Kamdar, F., and Garry, D.J. (2016). Dystrophin-Deficient Cardiomyopathy. J. Am. Coll. Cardiol. *67*, 2533–2546.

13. McNally, E.M. (2007). New approaches in the therapy of cardiomyopathy in muscular dystrophy. Annu. Rev. Med. *58*, 75–88.

14. Yue, Y., Binalsheikh, I.M., Leach, S.B., Domeier, T.L., and Duan, D. (2016). Prospect of gene therapy for cardiomyopathy in hereditary muscular dystrophy. Expert Opin. Orphan Drugs *4*, 169–183.

15. Lai, Y., and Duan, D. (2012). Progress in gene therapy of dystrophic heart disease. Gene Ther. *19*, 678–685.

16. Wasala, N.B., Bostick, B., Yue, Y., and Duan, D. (2013). Exclusive skeletal muscle correction does not modulate dystrophic heart disease in the aged mdx model of Duchenne cardiomyopathy. Hum. Mol. Genet. *22*, 2634–2641.

17. Prosser, B.L., Ward, C.W., and Lederer, W.J. (2011). X-ROS signaling: rapid mechano-chemo transduction in heart. Science *333*, 1440–1445.

18. Lai, Y., Zhao, J., Yue, Y., Wasala, N.B., and Duan, D. (2014). Partial restoration of cardiac function with ΔPDZ nNOS in aged mdx model of Duchenne cardiomyopathy. Hum. Mol. Genet. *23*, 3189–3199.

19. Nakamura, A., Harrod, G.V., and Davies, K.E. (2001). Activation of calcineurin and stress activated protein kinase/p38-mitogen activated protein kinase in hearts of utrophin-dystrophin knockout mice. Neuromuscul. Disord. *11*, 251–259.

20. Nakamura, A., Yoshida, K., Takeda, S., Dohi, N., and Ikeda, S. (2002). Progression of dystrophic features and activation of mitogen-activated protein kinases and calcineurin by physical exercise, in hearts of mdx mice. FEBS Lett. *520*, 18–24.

21. Wasala, N.B., Yue, Y., Lostal, W., Wasala, L.P., Niranjan, N., Hajjar, R.J., Babu, G.J., and Duan, D. (2020). Single SERCA2a Therapy Ameliorated Dilated Cardiomyopathy for 18 Months in a Mouse Model of Duchenne Muscular Dystrophy. Mol. Ther. *28*, 845–854.

22. Voit, A., Patel, V., Pachon, R., Shah, V., Bakhutma, M., Kohlbrenner, E., McArdle, J.J., Dell'Italia, L.J., Mendell, J.R., Xie, L.H., et al. (2017). Reducing sarcolipin expression mitigates Duchenne muscular dystrophy and associated cardiomyopathy in mice. Nat. Commun. *8*, 1068.

23. Huang, Z.P., Young Seok, H., Zhou, B., Chen, J., Chen, J.F., Tao, Y., Pu, W.T., and Wang, D.Z. (2012). CIP, a cardiac Isl1-interacting protein, represses cardiomyocyte hypertrophy. Circ. Res. *110*, 818–830.

24. Ahmady, E., Deeke, S.A., Rabaa, S., Kouri, L., Kenney, L., Stewart, A.F., and Burgon, P.G. (2011). Identification of a novel muscle A-type lamin-interacting protein (MLIP). J. Biol. Chem. *286*, 19702–19713.

25. Cattin, M.E., Wang, J., Weldrick, J.J., Roeske, C.L., Mak, E., Thorn, S.L., DaSilva, J.N., Wang, Y., Lusis, A.J., and Burgon, P.G. (2015). Deletion of MLIP (muscle-enriched A-type lamin-interacting protein) leads to cardiac hyperactivation of Akt/mammalian target of rapamycin (mTOR) and impaired cardiac adaptation. J. Biol. Chem. *290*, 26699–26714.

26. Huang, Z.P., Kataoka, M., Chen, J., Wu, G., Ding, J., Nie, M., Lin, Z., Liu, J., Hu, X., Ma, L., et al. (2015). Cardiomyocyte-enriched protein CIP protects against pathophysiological stresses and regulates cardiac homeostasis. J. Clin. Invest. *125*, 4122–4134.

27. Esslinger, U., Garnier, S., Korniat, A., Proust, C., Karakigas, G., Müller-Nurasyid, M., Empana, J.P., Morley, M.P., Perret, C., Stark, K., et al. (2017). Exome-wide association study reveals novel susceptibility genes to sporadic dilated cardiomyopathy. PLoS ONE *12*, e0172995.

28. Liu, J., Huang, Z.P., Nie, M., Wang, G., Silva, W.J., Yang, Q., Freire, P.P., Hu, X., Chen, H., Deng, Z., et al. (2020). Regulation of myonuclear positioning and muscle function by the skeletal muscle-specific CIP protein. Proc. Natl. Acad. Sci. USA *117*, 19254–19265.

29. Bridges, L.R. (1986). The association of cardiac muscle necrosis and inflammation with the degenerative and persistent myopathy of MDX mice. J. Neurol. Sci. *72*, 147–157.

30. Quinlan, J.G., Hahn, H.S., Wong, B.L., Lorenz, J.N., Wenisch, A.S., and Levin, L.S. (2004). Evolution of the mdx mouse cardiomyopathy: physiological and morphological findings. Neuromuscul. Disord. *14*, 491–496.

31. Bostick, B., Yue, Y., Long, C., and Duan, D. (2008). Prevention of dystrophin-deficient cardiomyopathy in twenty-one-month-old carrier mice by mosaic dystrophin expression or complementary dystrophin/utrophin expression. Circ. Res. *102*, 121–130.

32. Blain, A.M., Greally, E., Laval, S.H., Blamire, A.M., MacGowan, G.A., and Straub, V.W. (2015). Assessment of ventricular function in mouse models of muscular dystrophy: a comparison of MRI with conductance catheter. Neuromuscul. Disord. *25*, 24–31.

33. Li, W., Liu, W., Zhong, J., and Yu, X. (2009). Early manifestation of alteration in cardiac function in dystrophin deficient mdx mouse using 3D CMR tagging. J. Cardiovasc. Magn. Reson. *11*, 40.

34. Van Erp, C., Loch, D., Laws, N., Trebbin, A., and Hoey, A.J. (2010). Timeline of cardiac dystrophy in 3-18-month-old MDX mice. Muscle Nerve *42*, 504–513.

35. Betts, C.A., Saleh, A.F., Carr, C.A., Muses, S., Wells, K.E., Hammond, S.M., Godfrey, C., McClorey, G., Woffindale, C., Clarke, K., et al. (2015). Implications for Cardiac Function Following Rescue of the Dystrophic Diaphragm in a Mouse Model of Duchenne Muscular Dystrophy. Sci. Rep. *5*, 11632.

36. Walcher, T., Steinbach, P., Spiess, J., Kunze, M., Gradinger, R., Walcher, D., and Bernhardt, P. (2011). Detection of long-term progression of myocardial fibrosis in Duchenne muscular dystrophy in an affected family: a cardiovascular magnetic resonance study. Eur. J. Radiol. *80*, 115–119.

37. Brüning, J.C., Michael, M.D., Winnay, J.N., Hayashi, T., Hörsch, D., Accili, D., Goodyear, L.J., and Kahn, C.R. (1998). A muscle-specific insulin receptor knockout exhibits features of the metabolic syndrome of NIDDM without altering glucose tolerance. Mol. Cell *2*, 559–569.

38. Matsushima, S., Kuroda, J., Ago, T., Zhai, P., Park, J.Y., Xie, L.H., Tian, B., and Sadoshima, J. (2013). Increased oxidative stress in the nucleus caused by Nox4 mediates oxidation of HDAC4 and cardiac hypertrophy. Circ. Res. *112*, 651–663.

39. Kuroda, J., Ago, T., Matsushima, S., Zhai, P., Schneider, M.D., and Sadoshima, J. (2010). NADPH oxidase 4 (Nox4) is a major source of oxidative stress in the failing heart. Proc. Natl. Acad. Sci. USA *107*, 15565–15570.

40. Matsushima, S., Kuroda, J., Zhai, P., Liu, T., Ikeda, S., Nagarajan, N., Oka, S., Yokota, T., Kinugawa, S., Hsu, C.P., et al. (2016). Tyrosine kinase FYN negatively regulates NOX4 in cardiac remodeling. J. Clin. Invest. *126*, 3403–3416.

41. Owen, J.B., and Butterfield, D.A. (2010). Measurement of oxidized/reduced glutathione ratio. Methods Mol. Biol. *648*, 269–277.

42. Ding, J., Chen, J., Wang, Y., Kataoka, M., Ma, L., Zhou, P., Hu, X., Lin, Z., Nie, M., Deng, Z.L., et al. (2015). Trbp regulates heart function through microRNA-mediated Sox6 repression. Nat. Genet. *47*, 776–783.

43. Gao, F., Kataoka, M., Liu, N., Liang, T., Huang, Z.P., Gu, F., Ding, J., Liu, J., Zhang, F., Ma, Q., et al. (2019). Therapeutic role of miR-19a/19b in cardiac regeneration and protection from myocardial infarction. Nat. Commun. *10*, 1802.

44. Bostick, B., Ghosh, A., Yue, Y., Long, C., and Duan, D. (2007). Systemic AAV-9 transduction in mice is influenced by animal age but not by the route of administration. Gene Ther. *14*, 1605–1609.

45. Campbell, K.P., and Kahl, S.D. (1989). Association of dystrophin and an integral membrane glycoprotein. Nature *338*, 259–262.

46. Molkentin, J.D., Lu, J.R., Antos, C.L., Markham, B., Richardson, J., Robbins, J., Grant, S.R., and Olson, E.N. (1998). A calcineurin-dependent transcriptional pathway for cardiac hypertrophy. Cell *93*, 215–228.

47. Wilkins, B.J., Dai, Y.S., Bueno, O.F., Parsons, S.A., Xu, J., Plank, D.M., Jones, F., Kimball, T.R., and Molkentin, J.D. (2004). Calcineurin/NFAT coupling participates in pathological, but not physiological, cardiac hypertrophy. Circ. Res. *94*, 110–118.

48. Ni, Y.G., Berenji, K., Wang, N., Oh, M., Sachan, N., Dey, A., Cheng, J., Lu, G., Morris, D.J., Castrillon, D.H., et al. (2006). Foxo transcription factors blunt cardiac hypertrophy by inhibiting calcineurin signaling. Circulation *114*, 1159–1168.

49. Berry, J.M., Le, V., Rotter, D., Battiprolu, P.K., Grinsfelder, B., Tannous, P., Burchfield, J.S., Czubryt, M., Backs, J., Olson, E.N., et al. (2011). Reversibility of adverse, calcineurin-dependent cardiac remodeling. Circ. Res. *109*, 407–417.

50. Heineke, J., Auger-Messier, M., Correll, R.N., Xu, J., Benard, M.J., Yuan, W., Drexler, H., Parise, L.V., and Molkentin, J.D. (2010). CIB1 is a regulator of pathological cardiac hypertrophy. Nat. Med. *16*, 872–879.

51. Beals, C.R., Clipstone, N.A., Ho, S.N., and Crabtree, G.R. (1997). Nuclear localization of NF-ATc by a calcineurin-dependent, cyclosporin-sensitive intramolecular interaction. Genes Dev. *11*, 824–834.

52. Aramburu, J., Garcia-Cózar, F., Raghavan, A., Okamura, H., Rao, A., and Hogan, P.G. (1998). Selective inhibition of NFAT activation by a peptide spanning the calcineurin targeting site of NFAT. Mol. Cell *1*, 627–637.

53. Aramburu, J., Yaffe, M.B., López-Rodríguez, C., Cantley, L.C., Hogan, P.G., and Rao, A. (1999). Affinity-driven peptide selection of an NFAT inhibitor more selective than cyclosporin A. Science *285*, 2129–2133.

54. Williams, C.R., and Gooch, J.L. (2014). Calcineurin Aβ regulates NADPH oxidase (Nox) expression and activity via nuclear factor of activated T cells (NFAT) in response to high glucose. J. Biol. Chem. *289*, 4896–4905.

55. Taigen, T., De Windt, L.J., Lim, H.W., and Molkentin, J.D. (2000). Targeted inhibition of calcineurin prevents agonist-induced cardiomyocyte hypertrophy. Proc. Natl. Acad. Sci. USA *97*, 1196–1201.

56. Heineke, J., and Molkentin, J.D. (2006). Regulation of cardiac hypertrophy by intracellular signalling pathways. Nat. Rev. Mol. Cell Biol. *7*, 589–600.

57. Serrano, A.L., and Muñoz-Cánoves, P. (2017). Fibrosis development in early-onset muscular dystrophies: Mechanisms and translational implications. Semin. Cell Dev. Biol. *64*, 181–190.

58. Moulin, M., and Ferreiro, A. (2017). Muscle redox disturbances and oxidative stress as pathomechanisms and therapeutic targets in early-onset myopathies. Semin. Cell Dev. Biol. *64*, 213–223.

59. Allen, D.G., Whitehead, N.P., and Froehner, S.C. (2016). Absence of Dystrophin Disrupts Skeletal Muscle Signaling: Roles of Ca2+, Reactive Oxygen Species, and Nitric Oxide in the Development of Muscular Dystrophy. Physiol. Rev. *96*, 253–305.

60. Dombernowsky, N.W., Ölmestig, J.N.E., Witting, N., and Kruuse, C. (2018). Role of neuronal nitric oxide synthase (nNOS) in Duchenne and Becker muscular dystrophies - Still a possible treatment modality? Neuromuscul. Disord. *28*, 914–926.

61. Russo, V., Papa, A.A., Williams, E.A., Rago, A., Palladino, A., Politano, L., and Nigro, G. (2018). ACE inhibition to slow progression of myocardial fibrosis in muscular dystrophies. Trends Cardiovasc. Med. *28*, 330–337.

62. Spurney, C.F., Knoblach, S., Pistilli, E.E., Nagaraju, K., Martin, G.R., and Hoffman, E.P. (2008). Dystrophin-deficient cardiomyopathy in mouse: expression of Nox4 and Lox are associated with fibrosis and altered functional parameters in the heart. Neuromuscul. Disord. *18*, 371–381.

63. Chevalier, M., Vermij, S.H., Wyler, K., Gillet, L., Keller, I., and Abriel, H. (2018). Transcriptomic analyses of murine ventricular cardiomyocytes. Sci. Data *5*, 180170.

64. Rogers, R.G., Fournier, M., Sanchez, L., Ibrahim, A.G., Aminzadeh, M.A., Lewis, M.I., and Marbán, E. (2019). Disease-modifying bioactivity of intravenous cardiosphere-derived cells and exosomes in mdx mice. JCI Insight *4*, e125754.

65. Kamdar, F., Das, S., Gong, W., Klaassen Kamdar, A., Meyers, T.A., Shah, P., Ervasti, J.M., Townsend, D., Kamp, T.J., Wu, J.C., et al. (2020). Stem Cell-Derived Cardiomyocytes and Beta-Adrenergic Receptor Blockade in Duchenne Muscular Dystrophy Cardiomyopathy. J. Am. Coll. Cardiol. *75*, 1159–1174.

66. Spurney, C.F. (2011). Cardiomyopathy of Duchenne muscular dystrophy: current understanding and future directions. Muscle Nerve *44*, 8–19.

67. Au, C.G., Butler, T.L., Sherwood, M.C., Egan, J.R., North, K.N., and Winlaw, D.S. (2011). Increased connective tissue growth factor associated with cardiac fibrosis in the mdx mouse model of dystrophic cardiomyopathy. Int. J. Exp. Pathol. *92*, 57–65.

68. Burelle, Y., Khairallah, M., Ascah, A., Allen, B.G., Deschepper, C.F., Petrof, B.J., and Des Rosiers, C. (2010). Alterations in mitochondrial function as a harbinger of cardiomyopathy: lessons from the dystrophic heart. J. Mol. Cell. Cardiol. *48*, 310–321.

69. Betts, C.A., McClorey, G., Healicon, R., Hammond, S.M., Manzano, R., Muses, S., Ball, V., Godfrey, C., Merritt, T.M., van Westering, T., et al. (2019). Cmah-dystrophin deficient mdx mice display an accelerated cardiac phenotype that is improved following peptide-PMO exon skipping treatment. Hum. Mol. Genet. *28*, 396–406.

70. Burgoyne, J.R., Mongue-Din, H., Eaton, P., and Shah, A.M. (2012). Redox signaling in cardiac physiology and pathology. Circ. Res. *111*, 1091–1106.

71. Morawietz, H. (2018). Cardiovascular protection by Nox4. Cardiovasc. Res. *114*, 353–355.

72. Zhang, M., Brewer, A.C., Schröder, K., Santos, C.X., Grieve, D.J., Wang, M., Anilkumar, N., Yu, B., Dong, X., Walker, S.J., et al. (2010). NADPH oxidase-4 mediates protection against chronic load-induced stress in mouse hearts by enhancing angiogenesis. Proc. Natl. Acad. Sci. USA *107*, 18121–18126.

73. Parsons, S.A., Millay, D.P., Sargent, M.A., Naya, F.J., McNally, E.M., Sweeney, H.L., and Molkentin, J.D. (2007). Genetic disruption of calcineurin improves skeletal muscle pathology and cardiac disease in a mouse model of limb-girdle muscular dystrophy. J. Biol. Chem. *282*, 10068–10078.

74. Chakkalakal, J.V., Harrison, M.A., Carbonetto, S., Chin, E., Michel, R.N., and Jasmin, B.J. (2004). Stimulation of calcineurin signaling attenuates the dystrophic pathology in mdx mice. Hum. Mol. Genet. *13*, 379–388.

75. Chakkalakal, J.V., Michel, S.A., Chin, E.R., Michel, R.N., and Jasmin, B.J. (2006). Targeted inhibition of Ca2+ /calmodulin signaling exacerbates the dystrophic phenotype in mdx mouse muscle. Hum. Mol. Genet. *15*, 1423–1435.

76. Bulfield, G., Siller, W.G., Wight, P.A., and Moore, K.J. (1984). X chromosome-linked muscular dystrophy (mdx) in the mouse. Proc. Natl. Acad. Sci. USA *81*, 1189–1192.

77. Grieger, J.C., Choi, V.W., and Samulski, R.J. (2006). Production and characterization of adeno-associated viral vectors. Nat. Protoc. *1*, 1412–1428.

78. Xing, W., Zhang, T.C., Cao, D., Wang, Z., Antos, C.L., Li, S., Wang, Y., Olson, E.N., and Wang, D.Z. (2006). Myocardin induces cardiomyocyte hypertrophy. Circ. Res. *98*, 1089–1097.

79. Trapnell, C., Pachter, L., and Salzberg, S.L. (2009). TopHat: discovering splice junctions with RNA-Seq. Bioinformatics *25*, 1105–1111.

80. Anders, S., Pyl, P.T., and Huber, W. (2015). HTSeq–a Python framework to work with high-throughput sequencing data. Bioinformatics *31*, 166–169.

81. Anders, S., and Huber, W. (2010). Differential expression analysis for sequence count data. Genome Biol. *11*, R106.